Author/s:
Peterson, TJ;Western, AW;Argent, RM

Title:
Analytical methods for ecosystem resilience: A hydrological investigation

Date:
2012-10-16

Citation:
Peterson, T. J., Western, A. W. & Argent, R. M. (2012). Analytical methods for ecosystem resilience: A hydrological investigation. WATER RESOURCES RESEARCH, 48 (10), https://doi.org/10.1029/2012WR012150.

Persistent Link:
https://hdl.handle.net/11343/297408

Analytical methods for ecosystem resilience: A hydrological investigation

T. J. Peterson,[1] A. W. Western,[1] and R. M. Argent[2]

Received 17 March 2012; revised 12 August 2012; accepted 2 September 2012; published 16 October 2012.

[1] In recent years a number of papers have quantitatively explored multiple steady states and resilience within a wide range of hydrological systems. Many have identified multiple steady states by conducting simulations from different initial state variables and a few have used the more advanced technique of equilibrium or limit cycle continuation analysis to quantify how the number of steady states may change with a single model parameter. However, like resilience investigations into other natural systems, these studies often omit explanation of these fundamental resilience science techniques; rely on complex numerical methods rather than analytical methods; and overlook use of more advanced techniques from nonlinear systems mathematics. In the interests of wider adoption of advanced resilience techniques within hydrology, and advancing resilience science more broadly, this paper details fundamental methods for quantitative resilience investigations. Using a simple model of a spatially lumped unconfined aquifer, one and two parameter continuation analysis was undertaken algebraically. The shape of each steady state attractor basin was then quantified using Lyapunov stability curves derived at a range of precipitation rates, but was found to be inconsistent with the resilience behavior demonstrated by stochastic simulations. Most notably, and contrary to standard resilience concepts, the switching between steady states from wet or dry periods (and vice versa) did not occur by crossing of the threshold between the steady states. It occurred by exceedance of the two steady-state domain, producing a counterclockwise hysteresis loop. Additionally, temporary steady states were identified that could not have been detected using equilibrium continuation with a constant forcing rate. By combining these findings with the Lyapunov stability curves, new measures of resilience were developed for endogenous disturbances to the model and for the recovery from disturbances exogenous to the model.

Citation: Peterson, T. J., A. W. Western, and R. M. Argent (2012), Analytical methods for ecosystem resilience: A hydrological investigation, *Water Resour. Res.*, *48*, W10531, doi:10.1029/2012WR012150.

1. Introduction

[2] Over recent years, a number of hydrological studies have investigated multiple steady states [*Dent et al.*, 2002; *Anderies*, 2005; *D'Odorico et al.*, 2011; *D'Odorico and Porporato*, 2004; *Heffernan*, 2008; *Hilt et al.*, 2011; *Peterson et al.*, 2009a; *Rennermalm et al.*, 2010; *Ridolfi et al.*, 2006; *Runyan and D'Odorico*, 2010]. For those using physical based models, different quasi-equilibrium states and fluxes can emerge for one set of parameters and forcing, depending on the initial conditions. Between two steady states is a threshold, and the state variable distance to it from a steady state is a measure of the cumulative disturbance the system state can withstand before switching steady states. Often, this *distance* is adopted as the measure of a state's resilience (see section 2.2 of *Peterson* [2009], for a detailed review). For the multiple steady states to have the potential to emerge the system must have a positive biophysical feedback, but the emergence of the multiple steady states depends upon the strength of this feedback relative to the forcing. These concepts, and associated methods, draw heavily from the field of ecosystem resilience; where *Holling* [1973] defined resilience as the magnitude of the disturbance that a system can absorb without undergoing a regime shift, while *Scheffer et al.* [2001] states that a sufficiently severe perturbation of an ecosystem state may bring the system into the basin of attraction of another state.

[3] The potential importance of resilience concepts to hydrology has been highlighted in a number of reviews [*Rodriguez-Iturbe et al.*, 2007; *Dent et al.*, 2002; *Asbjornsen et al.*, 2011]; and hydrological modeling has been criticized for often implicitly assuming no positive feedbacks, and the existence of only one steady state, and thus assuming the system to be infinitely resilient to, say, climatic disturbances [*Peterson et al.*, 2009a]. While the field of ecosystem

[1]Department of Infrastructure Engineering, University of Melbourne, Melbourne, Victoria, Australia.
[2]Climate and Water Division, Bureau of Meteorology, Melbourne, Victoria, Australia.

Corresponding author: T. J. Peterson, Department of Infrastructure Engineering, University of Melbourne, Melbourne, Vic 3010, Australia. (timjp@unimelb.edu.au)

0043-1397/12/2012WR012150

resilience has been modeling multiple steady state systems since *Holling* [1973] and *May* [1977], only recently have hydrologists begun to numerically explore these concepts. Quantitative investigations of multiple hydrological attractors have been undertaken into vegetation-soil moisture [*D'Odorico et al.*, 2005; *Guttal and Jayaprakash*, 2007; *D'Odorico et al.*, 2008]; unconfined aquifer-vegetation interactions [*Peterson*, 2009; *Peterson et al.*, 2009a; *Anderies*, 2005; *Ridolfi et al.*, 2006; *Runyan and D'Odorico*, 2010]; wetlands [*D'Odorico et al.*, 2011; *Heffernan*, 2008]; and peatlands [*Rennermalm et al.*, 2010]. Like quantitative ecosystem resilience studies, many of these have ignored the spatial dimension. Recently, a spatial dimension has been incorporated into studies of soil moisture vegetation [*Guttal and Jayaprakash*, 2009; *van Nes and Scheffer*, 2005; *Dakos et al.*, 2010; *van de Koppel and Rietkerk*, 2004; *von Hardenberg et al.*, 2001]; groundwater flow [*Peterson et al.*, 2009a, 2009b]; interconnected lakes [*Hilt et al.*, 2011]; and lake nutrients [*Serizawa et al.*, 2009] to reveal complex dynamics not apparent from the l-D modeling. Despite the appeal of these concepts and the emergence of complex behavior from simple models, very few studies have undertaken field investigations of multiple hydrological attractors [*D'Odorico and Porporato*, 2004; *Heffernan*, 2008].

[4] To quantify the steady states (henceforth referred to as *attractors*) within a model, *Ludwig et al.* [1997] detailed a number of fundamental methods. A simple method is to conducted time-integration simulations from very different initial state variable values using nonstochastic forcing [e.g., *van Nes and Scheffer*, 2005; *Peterson et al.*, 2009b]. If the simulations converge to different steady states then multiple attractors exist. However, while simple to implement, this technique cannot easily identify the threshold between the attractors (henceforth referred to as *repellor*) and is cumbersome for exploring how the number of attractors change with a model parameter. A more advanced technique, called equilibrium or limit cycle continuation analysis or codim 0 bifurcation [*Kuznetsov*, 2004], has been adopted by some to quantify how the number of attractors change with a single model parameter [*Peterson*, 2009; *Ridolfi et al.*, 2006; *Runyan and D'Odorico*, 2010; *Ludwig et al.*, 1997]. It is a powerful technique for understanding complex nonlinear model behavior but very often it is undertaken using complex numerical methods, such as that of *Dhooge et al.* [2003], that render the concept opaque to most readers [e.g., *Peterson et al.*, 2009a]. An exception is that by *Ludwig et al.* [1997], in which two ecosystems are modeled by single ordinary differential equations (ODE) and the ODEs are analytically rearranged to quantify the attractor and repellors with a change in a model parameter. While being a worthy and transparent example of one-parameter equilibrium continuation analysis, there remains a considerable gap between the broader mathematics of continuation analysis [*Kuznetsov*, 2004] and those applied to resilience science. Recently, more advanced studies have quantified the number of attractors in two parameter space; however, the methods are often insufficiently detailed or require repeated time-integration simulations from differing initial conditions and parameter combinations [*van de Koppel and Rietkerk*, 2004; *van Nes and Scheffer*, 2005; *Møller et al.*, 2009; *Anderies et al.*, 2006], rather than formal two-parameter continuation methods. To encourage wider application within hydrology, this paper presents an analytical demonstration of one and two-parameter continuation analysis of a l-D ODE model for an unconfined aquifer. The shape of each attractor basin is then quantified using a method based on Lyapunov stability curves and the results compared against those from simulations under stochastic forcing. New insights into the switching between attractors are identified and then drawn upon to propose new measures of resilience. While the l-D groundwater model is very simple, relative to both conventional groundwater models and other ecosystem resilience models, this simplicity allowed the clear demonstration and development of a wide range of resilience analysis methods. Some of the methods may be problematic to apply to more complex models, but the authors hope that the clear presentation of resilience techniques will encourage adoption of resilience concepts and techniques within hydrology and expand the tools available to resilience scientists.

2. Methods

[5] In the following, the ODE model is detailed, after which analytical methods for quantifying the attractors in one and two parameter dimensions are demonstrated. Following this, methods for quantifying the shape of attractor basins are detailed; after which the validity of this method is assessed against simulations using stochastic annual forcing.

2.1. Model Description

[6] The ODE model simulates a single lumped unconfined aquifer in which groundwater recharge is estimated parametrically as a function of depth to water table, annual rainfall and potential evapotranspiration (see Figure 1 for a diagram of the conceptual model). The upper catchment and aquifer basement are no-flow and the lower catchment has a fixed head. Central to the model, and the potential for multiple attractors, is the parametric estimate of net recharge as a function of the depth to water table. Net recharge is the sum of evaporative loss from the water table and gross recharge. The evaporative loss approaches zero when the water table is deep and approaches a climatic maximum when at the surface. The gross recharge is defined in an unusual way in that it can be parameterized to increase as the water table approaches the surface. This allowed representation of reduced transpiration as a saline water table approaches the surface, which produced a positive feedback and the potential for multiple attractors [*Peterson*, 2009; *Peterson et al.*, 2009a; *Anderies*, 2005]. By algebraically defining fluxes for groundwater outflow and recharge, a single ordinary differential equation for the water table head, h [L], was formed:

$$AS\frac{dh}{dt} = -k_{sat}wb\frac{\partial h}{\partial x} + R_{net}, \tag{1}$$

where A [L^2] is a parameter for the modeled catchment area; S is a dimensionless parameter for the aquifer specific yield; k_{sat} [L T^{-1}] is a parameter for the aquifer saturated lateral hydraulic conductivity; w [L] is a parameter for the catchment width; b [L] is a variable for the saturated thickness of the aquifer; h [L] is a state variable for the elevation of the water table; x [L] is a parameter for the

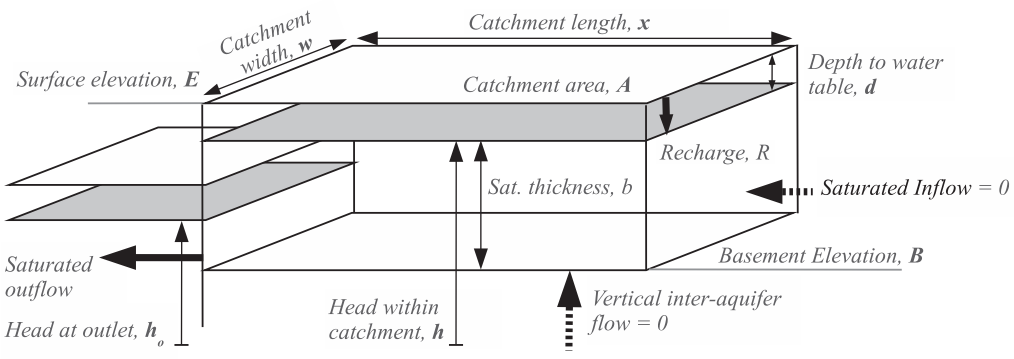

Figure 1. Schematic of the simple lumped groundwater model. Model parameters are labeled as bold letters. Model fluxes are depicted by thick lines and fluxes assumed to be zero are depicted by thick dashed lines.

catchment length; and R_{net} [L T^{-1}] is the net recharge estimated as recharge to the water table minus evaporation from the water table.

[7] To facilitate analytical continuation analysis, the model was simplified by approximating the partial derivative $\frac{\partial h}{\partial x}$ with the finite difference $\frac{h-h_o}{0.5x}$ (where h is taken as at the center of the study area, hence the multiplication of x by 0.5). Replacement of $\frac{2k_{sat}w}{x}$ with an aquifer conductance parameter, C_{aq}, then gives

$$AS\frac{dh}{dt} = \frac{k_{sat}w}{x}(h-B)(h-h_o) + R_{net}, \tag{2}$$

$$AS\frac{dh}{dt} = C_{aq}(h-B)(h-h_o) + R_{net}, \tag{3}$$

where h_o [L] is a parameter for the aquifer head elevation at the catchment outlet; and B [L] is a parameter for the elevation of the aquifer basement. To further simplify, the elevation of the aquifer basement was set to zero and the above bracketed terms were expanded to the following:

$$AS\frac{dh}{dt} = C_{aq}(h^2 - h_o h) + R_{net}. \tag{4}$$

Restructuring the state variable from head, h, to depth below surface, D [L], and then simplifying by substituting for constants gives

$$AS\frac{dD}{dt} = C_{aq}\left[(E-D)^2 - h_o(E-D)\right] - R_{net}, \tag{5}$$

$$AS\frac{dD}{dt} = C_{aq}(D^2 + \alpha D + \beta) - R_{net}, \tag{6}$$

where E [L] is a parameter for the elevation of the land surface; and the model constants are as follows:

$$C_{aq} = \frac{2k_{sat}w}{x}, \tag{7}$$

$$h = E - D, \tag{8}$$

$$\alpha = h_o - 2E, \tag{9}$$

$$\beta = E^2 - h_o E. \tag{10}$$

Net recharge, R_{net}, was modeled as gross recharge minus evaporative loss from the water table. Both gross recharge and evaporation from the water table increase as the water table rises toward the surface. A simple equation capturing these dynamics is

$$R_{net} = A\left(\sqrt{\frac{\max(P-r_3,0)}{r_1}}e^{-r_2 D} - PETe^{-c_1 D}\right), \tag{11}$$

where P [L T^{-1}] is the annual precipitation; r_3 [L T^{-1}] is a parameter for the precipitation at which recharge commences; r_1 is a dimensionless parameter controlling the rate at which the maximum recharge increases with precipitation; r_2 [L^{-1}] is a parameter for the decay rate of recharge with increasing water table depth; PET [L T^{-1}] is the annual areal potential evaporation; and c_1 [L^{-1}] is a parameter for the decay rate of water table evaporation with increasing water table depth. To illustrate the behavior of the square root coefficient, Figure 2a shows the calculated recharge for a depth to water table of 2 m, at five values of r_1 when r_3 equals 100 mm yr^{-1}. It shows gross recharge to occur only when annual precipitation is greater than r_3, above which recharge increases rapidly with precipitation and then slows at higher precipitation rates. It also shows this rate of increase in gross recharge to be inversely proportional to r_1. To illustrate the simulated dependency of recharge on depth to water table, Figure 2b shows the net recharge, gross recharge and evaporation as a function of depth to water table. To complete the differential equation, equation (11) was substituted into equation (6) for R_{net} to give

$$AS\frac{dD}{dt} = C_{aq}(D^2 + \alpha D + \beta) - A\left(\sqrt{\frac{\max(P-r_3,0)}{r_1}}e^{-r_2 D} - PETe^{-c_1 D}\right). \tag{12}$$

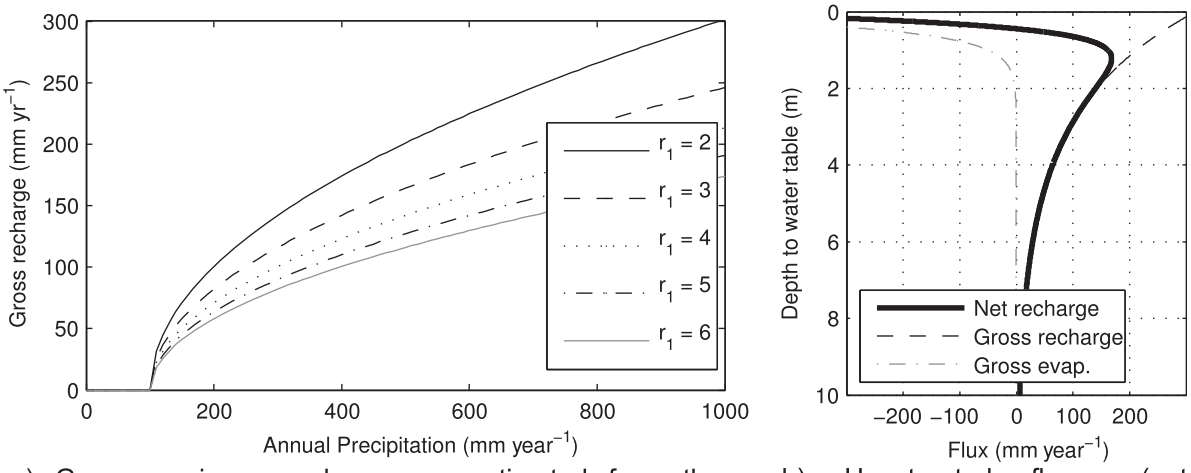

a) Gross maximum recharge, as estimated from the square-root term within equation 11, for a depth to water table of two meters and r_3 of 100 mm year^{-1}.

b) Unsaturated fluxes (net recharge, gross recharge, gross evaporation) for r_1 = 4, r_2 = 0.4 and r_3= 100 mm.

Figure 2. Example plots of gross maximum recharge and unsaturated fluxes.

[10] In the investigation of equation (12), the catchment area was set to a unit area of 1 km^2 and the catchment length, x, was assumed twice as much as the catchment width, which for a unit area catchment makes $x = \sqrt{2}$ km. The parameter for the head at the catchment outlet, h_o, was set to 2 meters below the land surface, E, minus a saturated hydraulic gradient of 0.0015 over a length of $\frac{x}{2}$ km. These simplifications resulted in the following equations for the constants:

$$C_{aq} = \frac{2k_{sat}w}{2w} = k_{sat}, \tag{13}$$

$$h_o = E - 0.0015\frac{\sqrt{2}}{2}. \tag{14}$$

Table 1 details the assigned values for all model parameters.

2.2. Steady State Estimation of Attractors

[11] A very simple method for identifying multiple attractors is to run the model from a wide range of initial state variable values, each using identical nonstochastic forcing. If the simulations from any of the initial conditions converge to a differing state variable value, then multiple attractors are likely to exist. This technique, while easily applied to most existing models, is limited to investigating only one parameter set at a time and by the requirement to use nonstochastic forcing, the latter complicating its application to rainfall-runoff modeling. Furthermore, the simulation should always be of sufficient duration to ensure that the solutions are attractors and not nonhyperbolic equilibrium.

[12] In this application, the above model was ran from 50 values for initial depth to water table from 0 to 12 meters. The mean annual climate forcing was applied to each year of each simulation. The model was solved using the MATLAB implicit variable time step solver *ode15s* [*Shampine and Reichelt*, 1997]. While the attractors could have been identified using only two initial conditions (with each at a different physically limit of the state variable), the 50 initial conditions were undertaken to provide an approximation of the repellor.

Table 1. Model Parameters

Parameter Name	Value
Conductance for lateral groundwater flow, C_{aq} (m yr^{-1})	700
Boundary water table head, h_o (m)	17.998
Land surface elevation, E (m)	20.0
Aquifer basement elevation, B (m)	0.0
Surface area, A (m^2)	1
Maximum recharge scalar, r_1	0.2
Rate of decay of recharge with D, r_2 (m^{-1})	0.4
Rainfall loss, r_3 (m yr^{-1})	0.1
Rate of increase of evaporation with D, c_1 (m^{-1})	3.0
Annual mean precipitation, P (m yr^{-1})	0.5
Annual mean areal potential evaporation, PET (m yr^{-1})	1.0

2.3. Equilibrium Continuation

[13] The analytical equilibrium continuation equation was derived for the aquifer conductance parameter C_{aq} by letting $\frac{dD}{dt} = 0$, and rearranging to an explicit equation for C_{aq}:

$$0 = C_{aq}(D^2 + \alpha D + \beta) - A\left(\sqrt{\frac{\max(P - r_3, 0)}{r_1}}e^{-r_2 D} - PETe^{-c_1 D}\right), \tag{15}$$

$$C_{aq} = \frac{A\left(\sqrt{\frac{\max(P-r_3,0)}{r_1}}e^{-r_2 D} - PETe^{-c_1 D}\right)}{D^2 + \alpha D + \beta}. \tag{16}$$

The stability of an equilibrium continuation point at water table depth, D, was determined by its eigenvalue, where negative real eigenvalues are point attractors and positive real values are point repellors. The simplicity of equation (12)

makes calculation of its eigenvalues straightforward. Further details are below:

$$\frac{d}{dD}\left(AS\frac{dD}{dt}\right) = C_{aq}(2D+\alpha) - A\left(-r_2\sqrt{\frac{\max(P-r_3,0)}{r_1}}e^{-r_2D} + c_1PETe^{-c_1D}\right). \tag{17}$$

To quantify the state-space location of attractors and the repellor, depth to water table values from zero to the depth of the aquifer basement were input into equation (16). This gave the corresponding value of aquifer conductance, C_{aq}, at which the aquifer would be at equilibrium. To determine the stability of these equilibrium points, the depth to water table and corresponding aquifer conductance were input to equation (17). An equilibrium continuation plot was then produced by plotting C_{aq} on the x axis against D on the y axis. This was undertaken for three values of the recharge decay parameter, r_2.

2.4. Fold-Point Continuation

[16] Points at which the eigenvalue (from equation (17)) equals zero denote bifurcation points. For this investigation, this denotes a change in the number of attractors with a change in C_{aq} and such points are called *fold points*. Equilibrium continuation using equation (16) results in two-fold points, each at a different value of C_{aq} (see Figure 5). Fold-point continuation allows the mapping, in two-parameter space, of the region of one and two attractors [*Kuznetsov*, 2004]. Within many bifurcation texts fold-point continuation is referred to as one form of codim 1 bifurcation [*Kuznetsov*, 2004]. Here fold-point continuation was used to aid the understanding of the interaction between recharge and aquifer lateral discharge on the emergence of one and two attractors. Specifically, the parameters investigated were those for the decay of recharge with depth, r_2, and for aquifer conductance, C_{aq}. The fold-point continuation was undertaken by, first, equating the right-hand side of equation (17) to 0 and then rearranging to an explicit equation for C_{aq}:

$$C_{aq} = \frac{A\left(-r_2\sqrt{\frac{\max(P-r_3,0)}{r_1}}e^{-r_2D} + c_1PETe^{-c_1D}\right)}{2D+\alpha}. \tag{18}$$

As fold points are also at an equilibrium, that is, $\frac{dD}{dt} = 0$, equation (18) can be equated to the equilibrium continuation equation for C_{aq}, equation (16), to give

$$\frac{A\left(\sqrt{\frac{\max(P-r_3,0)}{r_1}}e^{-r_2D} - PETe^{-c_1D}\right)}{D^2+\alpha D+\beta} = \frac{A\left(-r_2\sqrt{\frac{\max(P-r_3,0)}{r_1}}e^{-r_2D} + c_1PETe^{-c_1D}\right)}{2D+\alpha}. \tag{19}$$

Rearranging to a simpler form,

$$\sqrt{\frac{\max(P-r_3,0)}{r_1}}e^{-r_2D} - PETe^{-c_1D} = \left(-r_2\sqrt{\frac{\max(P-r_3,0)}{r_1}}e^{-r_2D} + c_1PETe^{-c_1D}\right)\frac{D^2+\alpha D+\beta}{2D+\alpha}. \tag{20}$$

Substituting constants for fixed terms (i.e., those independent of r_2) and rearranging to simplify,

$$\Gamma_3 + \sqrt{\frac{P-r_3}{r_1}}e^{-r_2D} = \left[\Gamma_2 - r_2\sqrt{\frac{\max(P-r_3,0)}{r_1}}e^{-r_2D}\right]\Gamma_1 \tag{21}$$

$$\sqrt{\frac{\max(P-r_3,0)}{r_1}}(1+\Gamma_1r_2)e^{-r_2D} = \Gamma_1\Gamma_2 - \Gamma_3, \tag{22}$$

$$(1+\Gamma_1r_2)e^{-r_2D} = \frac{\Gamma_1\Gamma_2-\Gamma_3}{\sqrt{\frac{\max(P-r_3,0)}{r_1}}}, \tag{23}$$

$$(1+r_2\Gamma_1)e^{-r_2D} = \Gamma_4, \tag{24}$$

where

$$\Gamma_1 = \frac{D^2+\alpha D+\beta}{2D+\alpha}, \tag{25}$$

$$\Gamma_2 = c_1PETe^{-c_1D}, \tag{26}$$

$$\Gamma_3 = -PETe^{-c_1D}, \tag{27}$$

$$\Gamma_4 = \frac{\Gamma_1\Gamma_2-\Gamma_3}{\sqrt{\frac{\max(P-r_3,0)}{r_1}}}. \tag{28}$$

Equation (24) cannot be rearranged to an explicit equation for r_2. However, an explicit equation can be derived by rearranging to the *Lambert W Function* form of $x = We^W$ and solving for W. To bring equation (24) into this form, both sides were first multiplied by D, then divided by Γ_1, then multiplied $-\frac{D}{\Gamma_1}e^{-\frac{D}{\Gamma_1}}$:

$$-\Gamma_4D = (-r_2D\Gamma_1 - D)e^{-r_2D}, \tag{29}$$

$$-\frac{\Gamma_4D}{\Gamma_1} = \frac{-r_2D\Gamma_1-D}{\Gamma_1}e^{-r_2D}, \tag{30}$$

$$-\frac{\Gamma_4D}{\Gamma_1}e^{\frac{-D}{\Gamma_1}} = \frac{-r_2D\Gamma_1-D}{\Gamma_1}e^{-r_2D}e^{\frac{-D}{\Gamma_1}}. \tag{31}$$

Simplifying the two right-hand side exponential terms of equation (31) resulted in an equation of the form $x = We^W$, where $W = \frac{-r_2D\Gamma_1-D}{\Gamma_1}$:

$$-\frac{\Gamma_4D}{\Gamma_1}e^{\frac{-D}{\Gamma_1}} = \frac{-r_2D\Gamma_1-D}{\Gamma_1}e^{\frac{-r_2D\Gamma_1-D}{\Gamma_1}}. \tag{32}$$

Using the special mathematical function *Lambert W* [*Corless et al.*, 1996], a numerical estimate for W at x, which equals $-\frac{\Gamma_4D}{\Gamma_1}e^{\frac{-D}{\Gamma_1}}$, can be derived and equated to the explicit equation for W, namely $\frac{-r_2D\Gamma_1-D}{\Gamma_1}$:

$$\frac{-r_2 D\Gamma_1 - D}{\Gamma_1} = \mathrm{W}\left(-\frac{\Gamma_4 D}{\Gamma_1} e^{\frac{-D}{\Gamma_1}}\right), \tag{33}$$

Rearranging this gives an explicit equation for r_2:

$$r_2 = -\frac{\mathrm{W}\left(-\frac{D\Gamma_4}{\Gamma_1} e^{-\frac{D}{\Gamma_1}}\right)\Gamma_1 + D}{D\Gamma_1}, \tag{34}$$

[24] Fold-point continuation was undertaken by substituting values for D from zero to the depth of the aquifer basement into equation (35) and calculating the corresponding value of r_2. Next, these values of D and r_2 were substituted into equation (18) to obtain C_{aq}. Together, these values of C_{aq} and r_2 enclose the parameter space of two attractors. However, a challenge in implementing equation (35) was that the Lambert W function has a complex component when $-\frac{D\Gamma_4}{\Gamma_1} e^{-\frac{D}{\Gamma_1}}$ is less than $exp(-1)$. This caused a failure at the upper C_{aq} fold-point value when r_2 was greater than or equal to 1.0. To produce a fold-point continuation result when $r_2 \geq 1$, the Lambert W value was approximated by linearly interpolating between $x = 0$ and $x = exp(-1)$, and the respective Lambert W values of negative one and zero. This resulted in the following equation for W. In implementation, this approximation was compared against the exact solution.

$$W(x) \simeq -\frac{D\Gamma_4}{\Gamma_1} e^{-\frac{D}{\Gamma_1}} e^1. \tag{35}$$

2.5. Lyapunov Estimation of Attractor Basin Shape

[25] Equilibrium continuation provides valuable insight into the cumulative disturbance a system can withstand before crossing the repellor and switching into an alternative attractor basin (see Figure 5). However, the resilience of a system is also a function of more subtle features of the attractor basin shape not quantified by equilibrium continuation. As conceptually demonstrated by *Walker et al.* [2004] and *Guttal and Jayaprakash* [2007], the resilience of a system is also a function of the relative *depth* of an attractor basin. A more subtle feature is the shape of the basin, which could vary widely, including being parabolic; having a flat broad bottom and steep sides; or having a *semistable* point arising from a nonhyperbolic equilibrium. Quantifying the attractor basin shape potentially provides insights into the probability of the system being within a given attractor basin or switching basins and the expected temporal dynamics under stochastic forcing. However, despite these potential benefits, to the author's knowledge, there have been no techniques applied or developed for quantifying the attractor shape for resilience investigations.

[26] In an effort to quantify the shape, one option would be to add contours of the state variable rate of change to the equilibrium continuation plot. Figure 3 shows an example, undertaken by deriving the analytical equilibrium (equation (16)) with $\frac{dD}{dt}$ set to increments of 0.2 m yr^{-1}. It shows a *steep* shallow attractor boundary near the land surface; more contours within the shallow attractor, which is thus likely to be of a *deeper* shape; and a near constant rate of change at C_{aq} of 700 m yr^{-1} when the depth to water table is 5 to 7 m. However, while visually useful, it cannot be directly used to quantify the shape for a given parameter set. This is because to simply take a vertical cross section through it for a given value of C_{aq} would require integration over time to produce a *depth* to the basin shape. That is, the *depth* of the basin would be given by the recovery time to the attractor. Considering that, for example, near the land surface the recovery time would be very rapid, such a method would incorrectly depict this attractor wall to be less *deep* than others requiring a considerably longer recovery time.

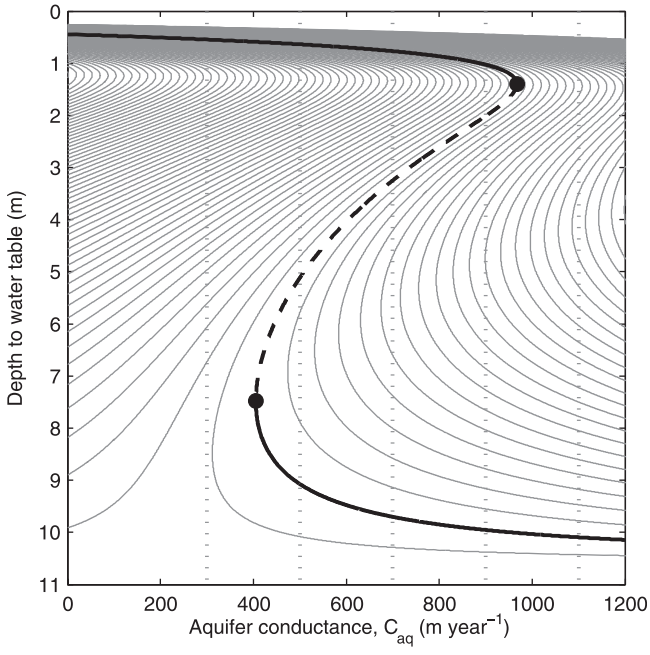

Figure 3. Equilibrium continuation plot with contours of $\frac{dD}{dt}$ at increments of 0.2 m yr^{-1} for the aquifer conductance, C_{aq}. Note, the solid thick black line denotes an attractor; the dashed thick black line denotes a repellor; each bullet denotes a fold point; the solid thick gray lines denote contours; and the dotted vertical lines indicate the values of C_{aq} at which the attractor basin shape is quantified within Figure 7.

[27] An alternative method is Lyapunov's second method for stability (*Lyapunov* [1992], translated from his 1892 Russian dissertation). It is widely used within control theory and facilitates identification of stable solutions to differential equations without solution of these equations via identification of a valid *energy function* (which often has no physical basis). Lyapunov's Stability Theorem gives a precise characterization of functions that qualify as *valid energy functions* in the vicinity of an attractor and requires that the *energy functions* decrease toward the attractor [*Sastry*, 1999]. From *Sastry* [1999], the basic theorem of Lyapunov states that when the energy function, $V(\lambda)$, is locally positive definite and $\frac{dV}{dt} \leq 0$ then the equilibrium point can be concluded as stable. That is, a scalar function, V, is sought which is greater than zero at all values of λ, except at $\lambda = 0$ where $V = 0$, and V declines with time when $\lambda > 0$. However, while a powerful theorem, multiple energy functions may satisfy these conditions for any given problem and, to the author's knowledge, no generally applicable method exists for finding valid Lyapunov functions. Furthermore, in this application the focus was on identifying

an energy function to characterize the shape of the attractor basins, and not on estimating the depth to water table of the attractors without solution of the differential equation model. Hence, a variant of the full model (i.e., equation (12)) was used, rather than a simpler energy function, as is often sought in Lyapunov stability investigations.

[28] In identifying a valid Lyapunov energy function for equation (12), the first step was to ensure $V(\lambda) = 0$ when $\lambda = 0$ by defining λ with reference to the lowest energy attractor. Therefore the Lyapunov variable, λ, was defined as

$$\lambda = D - \Delta, \tag{36}$$

where D [L], as before, is the depth to water table; and Δ is the depth to water table at an attractor or repellor from which the Lyapunov datum is to be defined. In this application, from a given value of C_{aq}, each attractor and repellor that existed was investigated as a possible datum.

[29] Next, the equilibrium continuation plots were used to provide some insight into the expected form of the Lyapunov function (see Figure 5). For a value of C_{aq} that has two attractors, say 700 m yr^{-1}, Figure 5b shows that there are three depth to water table values where $\frac{dD}{dt} = 0$. Consequently, a Lyapunov function should also have three depth to water values where $\frac{\partial V}{\partial \lambda} = 0$; an appropriate function for this is

$$\frac{\partial V}{\partial \lambda} = \frac{dD}{dt}\lambda^2. \tag{37}$$

To derive a Lyapunov function, the integral function for equation (37), $F(\lambda)$, was derived:

$$F = \int \frac{dD}{dt}\lambda^2 \, \partial\lambda, \tag{38}$$

$$F = -\frac{1}{AS}\left(\int \lambda^2 Q \, \partial\lambda - A\int \lambda^2 R_{net} \, \partial\lambda\right), \tag{39}$$

where, from section 2.1, the right-hand integrals of equation (39) can be derived as the following:

$$\begin{aligned}\int \lambda^2 Q \, \partial\lambda = C_{aq}\Bigg[&\frac{1}{5}D^5 + D^4\left(\frac{1}{4}\alpha - \frac{1}{2}\Delta\right) \\ &+ D^3\left(\Delta^{2/3} - \frac{2}{3}\alpha\Delta + \frac{1}{3}\beta\right) - D^2\left(\Delta\beta - \frac{1}{2}\alpha\Delta\right) \\ &+ \Delta^2\beta D\Bigg],\end{aligned} \tag{40}$$

$$\begin{aligned}\int \lambda^2 R_{net} \, \partial\lambda = &-r_2^{-2}\sqrt{\frac{\max(P - r_3, 0)}{r_1}} \\ &\left[r_2(\Delta^2 - 2\Delta D + D^2) - 2\Delta + 2D + \frac{2}{r_2}\right]\exp(-r_2 D) \\ &+ \frac{PET}{c_2^2}\left[c_2(\Delta^2 - 2\Delta D + D^2) - 2\Delta + 2D + \frac{2}{c_2}\right]\exp(-c_2 D),\end{aligned} \tag{41}$$

Using equation (39), the Lyapunov stability function, $V(\lambda)$, can be calculated from the minimum depth to water table of D_{min} to the maximum depth to water table of D_{max}. To meet the Lyapunov stability requirement that the energy equals zero at the lowest energy point, the integration constant, C, was derived by calculating F at each attractor and setting C to equal the negative of the attractor of minimum energy:

$$V = \int_{\lambda = D_{min} - \Delta}^{D_{max} - \Delta} \frac{dD}{dt} x \, \partial\lambda + C, \tag{42}$$

$$V = F(\lambda_b) - F(\lambda_a) + C. \tag{43}$$

2.6. Assessing Stochastic Model Dynamics

[32] The above methods have quantified the model behavior only under mean climate forcing. Considering that stochastic disturbances are a fundamental aspect of natural systems and central to most definitions of resilience, the behavior of the model under stochastic forcing warrants further investigation. To this end, two time-integration simulations with stochastic forcing were undertaken to demonstrate: the switching between attractors; assess whether this reflects the behavior expected for the shape of the attractor basins; and inform how stochastic forcing can cause a shift between attractors.

[33] Two stochastic annual precipitation series were derived using a simple autoregressive lag 1 model for skewed data. Following *Srikanthan et al.* [2002], the AR(1) model is of the form:

$$X_t = rX_{t-1} + (1 - r^2)^{1/2}\epsilon_t, \tag{44}$$

where X_t is the standardized rainfall in year t; r is the lag one autocorrelation coefficient; and ϵ the skewed random component of the AR(1) model. The annual rainfall amount was then obtained from

$$P_t = \overline{P} + sX_t, \tag{45}$$

where $\overline{P}$ is the mean annual precipitation; and s the standard deviation in the precipitation. The aforementioned inclusion of a skewed random component was adopted to produce years of extreme rainfall sufficient to cause a switching of attractor basins. This switching could have been achieved with a zero skew and very high variance, but this would have resulted in many years of zero rainfall. Following *Srikanthan et al.* [2002], the skewness was modeled using the following transformation:

$$\epsilon_t = \frac{2}{g_\epsilon}\left[\left(1 + \frac{g_\epsilon \eta_t}{6} - \frac{g_\epsilon^2}{36}\right)^3 - 1\right], \tag{46}$$

where η_t is the normally distributed random component with a mean of zero and unit variance; and g_ϵ is the skewness of

ϵ_t, related to the skewness in the nontransformed data, g, as follows:

$$g_\epsilon = \frac{1 - r^3}{(1 - r^2)^{3/2}} g. \quad (47)$$

In implementing the stochastic rainfall model, the parameters were as follows: $\overline{P}$ equaled 500 mm yr^{-1}; g equaled 2; r equaled 0.8; and s for stochastic series A and B equaled 500 mm yr^{-1} and 250 mm yr^{-1}, respectively. These parameters clearly represent an extremely variable and somewhat unrealistic climate but were chosen because they produced climate series that result in two types of switching between the attractor basins; namely repeated switching between the attractor basins (series A) and a single crossing of the repellor followed by persistence within the alternative attractor basin (series B). During the stochastic generation, if the large standard deviation caused a negative precipitation, the random number η_t was resampled until a nonnegative precipitation was produced. This truncation resulted in a slight reduction in the standard deviation of each series from that defined by the input standard deviation, s. Furthermore, to ensure the two series differed only in the standard deviation, identical random number sequences were used for each. In selecting a climate series, dozens of 250 year series were generated and model simulations were conducted until climate series were identified that clearly produced the desired two types of attractor basin switching.

[35] In solving the model, the MATLAB implicit variable time step solver *ode15s* [*Shampine and Reichelt*, 1997] was again used and the aquifer conductance, C_{aq}, was set to 700 m yr^{-1}. This value was chosen because the equilibrium continuation (see Figure 5b) indicates that at this value of C_{aq} both attractors exist and that the repellor is sufficiently close to both attractors that repeated switching between the attractor basins is likely. The initial depth to water table was taken as the steady state shallow attractor depth, as given in Figure 5b, when C_{aq} equals 700 m yr^{-1}. As a side note, differential equations that contain a positive feedback are often stiff; that is the state-variables may quickly switch from changing slowly to very rapidly with time. Numerical solution of such equations often require an implicit stiff solver, such as *ode15s*. Use of an explicit solver, such as variable time step Runge-Kutta, has been found to produce very unstable results that fail to simulate multiple attractors.

[36] The stochastic simulation results were then qualitatively assessed against the expected frequency of attractor basin switching from the Lyapunov estimates of attractor basin shape; where a basin of *shallow* depth would be expected to produce stochastic simulations that rapidly switch out of the attractor basin and conversely for a *deep* basin. To further consider how attractor basin switching occurs under stochastic forcing, a 3-D Lyapunov stability surface was then derived by calculating the Lyapunov stability (equation (43)) for precipitation rates of zero to 3000 mm yr^{-1} and C_{aq} of 700 m yr^{-1}. The two stochastic simulations were then overlain to inform how stochastic forcing causes a change of attractor basins.

[37] As a result of insights gained from the 3-D Lyapunov analysis, equilibrium continuation was also undertaken for the annual precipitation rate, rather than for C_{aq}. Using the same methodology as detailed within section 2.3, the following equilibrium continuation equation was derived:

$$P = r_1 e^{2r_2 D}\left[\frac{C_{aq}}{A}(D^2 + \alpha D + \beta) + PETe^{-c_1 D}\right]^2 + r_3, \quad (48)$$

where, because of the *max* term within equation (11), P is valid only when greater than or equal to r_3. In using this equation, C_{aq} was set to 1100 m yr^{-1}; at which the equilibrium continuation indicate only the deep attractor to exist. This value of C_{aq} was chosen to demonstrate inconsistencies between the equilibrium continuation results for C_{aq} and for precipitation. To force this model to a groundwater level approximately at the shallow attractor, a precipitation series of extreme variability was derived using the same parameters as above but with the standard deviation increased to 750 mm yr^{-1}. The results from the simulation were then analyzed by plotted them onto the precipitation equilibrium continuation plot.

3. Results and Discussion

3.1. Steady State Estimation of Attractors

[38] Figure 4 shows the time-integration solutions, using the mean annual precipitation, undertaken from 50 initial conditions. It shows convergence to two significantly different depth to water table values, with faster convergence to the shallow state. By noting the depth at which the simulations diverge, the depth to the water table of the repellor can also be estimated at 3 m. Clearly this method of

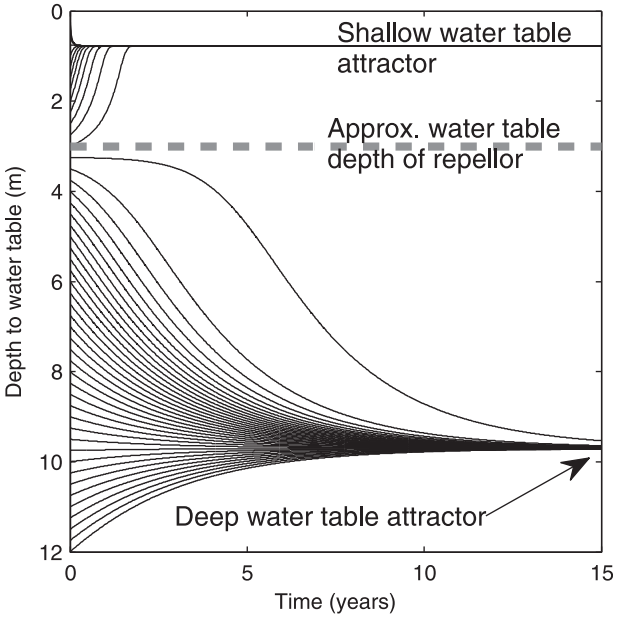

Figure 4. Time integration simulation of depth to water table from 50 initial depths undertaken to estimate the attractors and repellor. The aquifer conductance parameter, C_{aq}, was set to 700 m yr^{-1} and the recharge decay parameter, r_2, was set to 0.4 m^{-1}.

identifying attractors can be easily applied to very complex models with many state variables; however, for such models the repellor cannot be estimated. It is also important to ensure that the simulation duration is sufficient to avoid incorrect identification of a nonhyperbolic equilibrium (i.e., a *semistable* point) as an attractor. For such complex models, if the repellor needs to be identified then equilibrium continuation should be undertaken. While equilibrium continuation is only amenable to models with a continuous first derivative, it does provide efficient estimation of the change in the number of attractors with a change in one model parameter (or forcing).

3.2. Equilibrium Continuation

[39] Figure 5 presents water table equilibrium continuation plots for three values of the decay in gross recharge with depth to water table, r_2. The figures provide insight into the dependence of the number and location of attractors on the groundwater outflow rate and recharge. Figure 5b shows that two attractors emerge when C_{aq} is between 405 and 1397 m yr^{-1}. Above 1397 and below 405 only the deep attractor and shallow attractor exist, respectively. Figure 5a shows that decreasing r_2 from 0.4 to 0.23 m^{-1} shifts the two-attractor range to higher values of C_{aq} and significantly reduces the extent of the two-attractor range to between 1187 and 1276 m yr^{-1}. Figure 5c shows that increasing r_2 to 0.7 m^{-1} shifts the two-attractor range to lower values of C_{aq} and modestly reduces the extent to between 33 and 618 m yr^{-1}. With regard to the model behavior within the two-attractor range, a common measure of resilience is the distance between the attractor and the repellor. By this measure, a subtler aspect of the results is that the resilience of the deep water table attractor increases as r_2 increases, yet there is not a corresponding decrease in the resilience of the shallow attractor. Additionally, by this measure of resilience, Figure 5b shows that, for C_{aq}, the deep attractor has the greater resilience. However, Figure 4 shows the water table moves considerably more rapidly to the shallow than to the deep attractor which, conversely, indicates that the shallow attractor is the most resilient. This contradiction is due to the inability of equilibrium continuation to characterize the *shape* of each attractor basin.

3.3. Fold-Point Continuation

[40] Figure 6 presents the fold-point continuation results for C_{aq} against r_2 repeated at four values of boundary condition hydraulic gradient. It shows the parameter space over which two attractors emerge under mean climate forcing. Figure 6c shows the fold-point continuation results for the hydraulic gradient adopted in the previous sections, along with the fold points from equilibrium continuation. These points are in good agreement with the numerical approximation when r_2 is greater than 1.0, which indicates the numerical approximation to the Lambert *W* function is acceptable. Figure 6c also shows that two attractors can only exist if r_2 is greater than 0.19 m^{-1}. However, the emergence of two attractors when r_2 is greater than 0.19 m^{-1} is very dependent upon the interaction between the groundwater outflow rate and recharge decay rate. Figure 6c also delineates three regions of the C_{aq} and r_2 parameter space, where (1) only the shallow attractor emerges; (2) only the deep attractor emerges; and (3) both the shallow and the deep attractors emerge. The other three plots each show similar regions of the parameter space; however, it can be seen that as the hydraulic gradient increases, the area of the two-attractor parameter space increases; two attractors emerge at a lower recharge decay rate; and the area with only the shallow attractor contracts. Clearly, this delineation of the parameter space enhances understanding of model dynamics. For the scenario of a calibrated model with quantified parameter uncertainty, fold point continuation could provide a numerically efficient means of estimating the probability of two attractors existing. However, for all but the simplest of models an analytical method would be inappropriate. Most often a numerical fold-point continuation method, such as that of *MatCont* [*Dhooge et al.*, 2003], would be required.

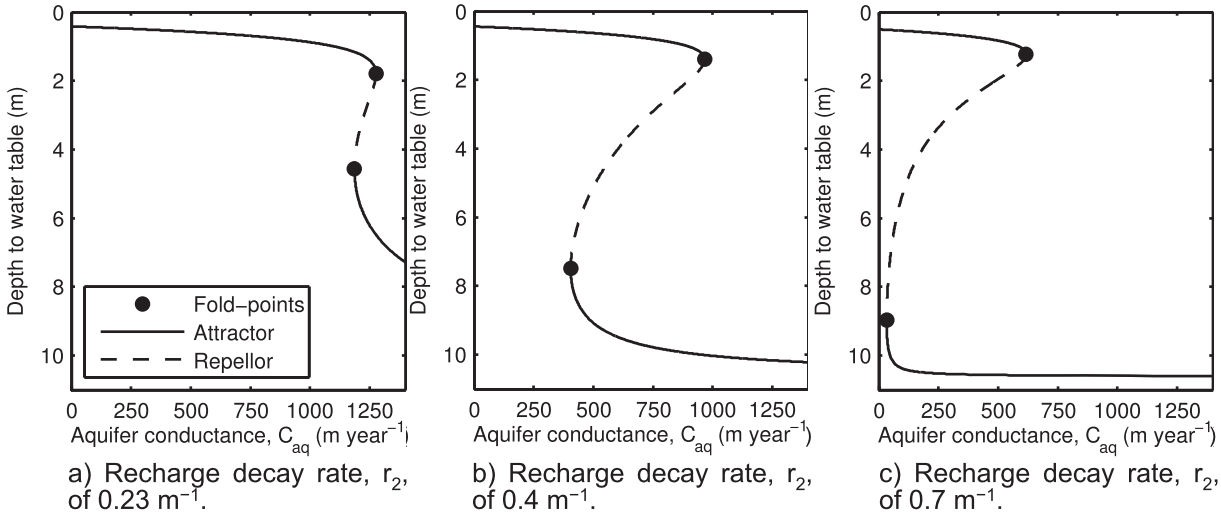

Figure 5. Equilibrium continuation results for depth to water table against the aquifer conductance parameter, C_{aq}.

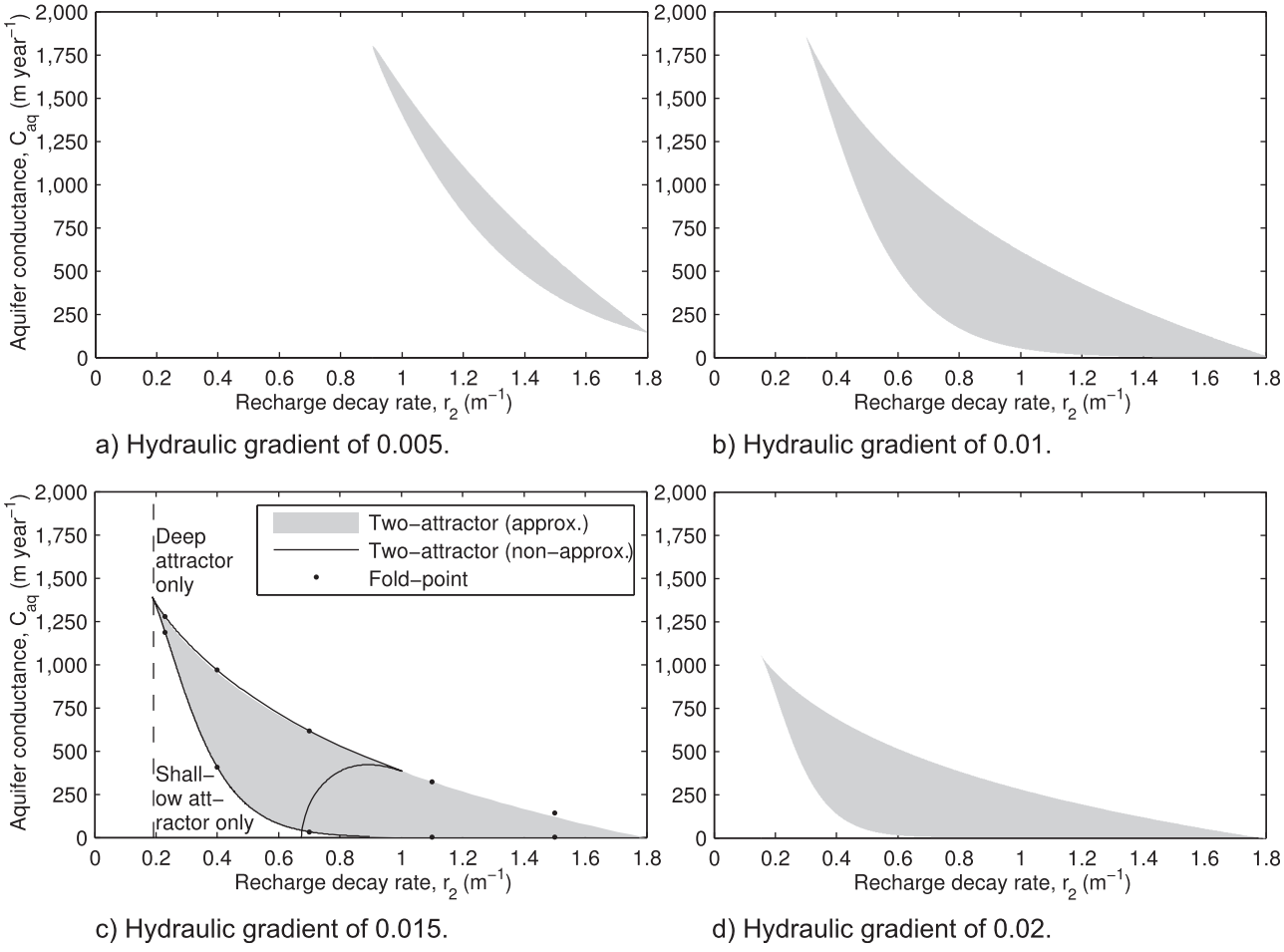

Figure 6. Fold-point continuation results for the aquifer conductance parameter, C_{aq}, and the parameter for the recharge decay rate with depth to water table, r_2, and repeated at four values of boundary condition head, h_o, (expressed as the hydraulic gradient). (a) Hydraulic gradient of 0.005; (b) hydraulic gradient of 0.01; (c) hydraulic gradient of 0.015; and (d) hydraulic gradient of 0.02. The gray region within each plot identifies the parameter space with two attractors. The black dots in Figure 6c identify the parameter space location of the fold points identified from equilibrium continuation. The dotted vertical line in Figure 6c delineates three additional parameter regions such that (1) above the gray region and to the right of the dotted line only the deep attractor exists; (2) below and to the right of the line only the shallow attractor exists; and (3) to the left of the line only one attractor exists for all values of C_{aq}. The black semicircle within Figure 6c is a numerical artifact resulting from the Lambert W function having a complex solution when $-\frac{D\Gamma_4}{\Gamma_1}e^{-\frac{D}{\Gamma_1}}$ is less than $exp(-1)$.

3.4. Lyapunov Estimation of Attractor Basin Shape

[41] Figure 7 shows the Lyapunov stability curves for the five values of C_{aq} denoted on the equilibrium continuation contour plot (Figure 3) repeated from the datum centered at the shallow attractor, repellor and deep attractor. If the datum does not exist for a given value of C_{aq} then its curve was not calculated. Key aspects are, first, that for any datum all equilibrium points were identified. For example, when the datum was set to the shallow attractor, the depth to water table of the repellor and deep attractor was estimated. This occurred because the model ODE was used within the Lyapunov stability function, rather than a simpler equation as is often adopted. A second key aspect of the plots is that the relative depth of each attractor basin depends upon the choice of datum. That is, generally the attractor furthest from the datum (as measured by depth to water table) had the deepest attractor basin. Considering that each stability curve satisfies the required Lyapunov conditions, choosing between them depends upon the nature of the problem.

[42] In this example, two aspects of the model give some guidance as to the choice of an appropriate stability curve. First, the exponential function for groundwater evaporation produces a strong negative feedback (as shown by the dense contours near to a zero depth within Figure 3). This indicates that the Lyapunov stability curve should be very steep between the shallow attractor and the land surface; a feature not shown in Figure 7 when the datum was set to the shallow attractor. Second, Figure 4 shows convergence of the water table to an attractor is most rapid when within the shallow attractor basin; a feature also evident from the

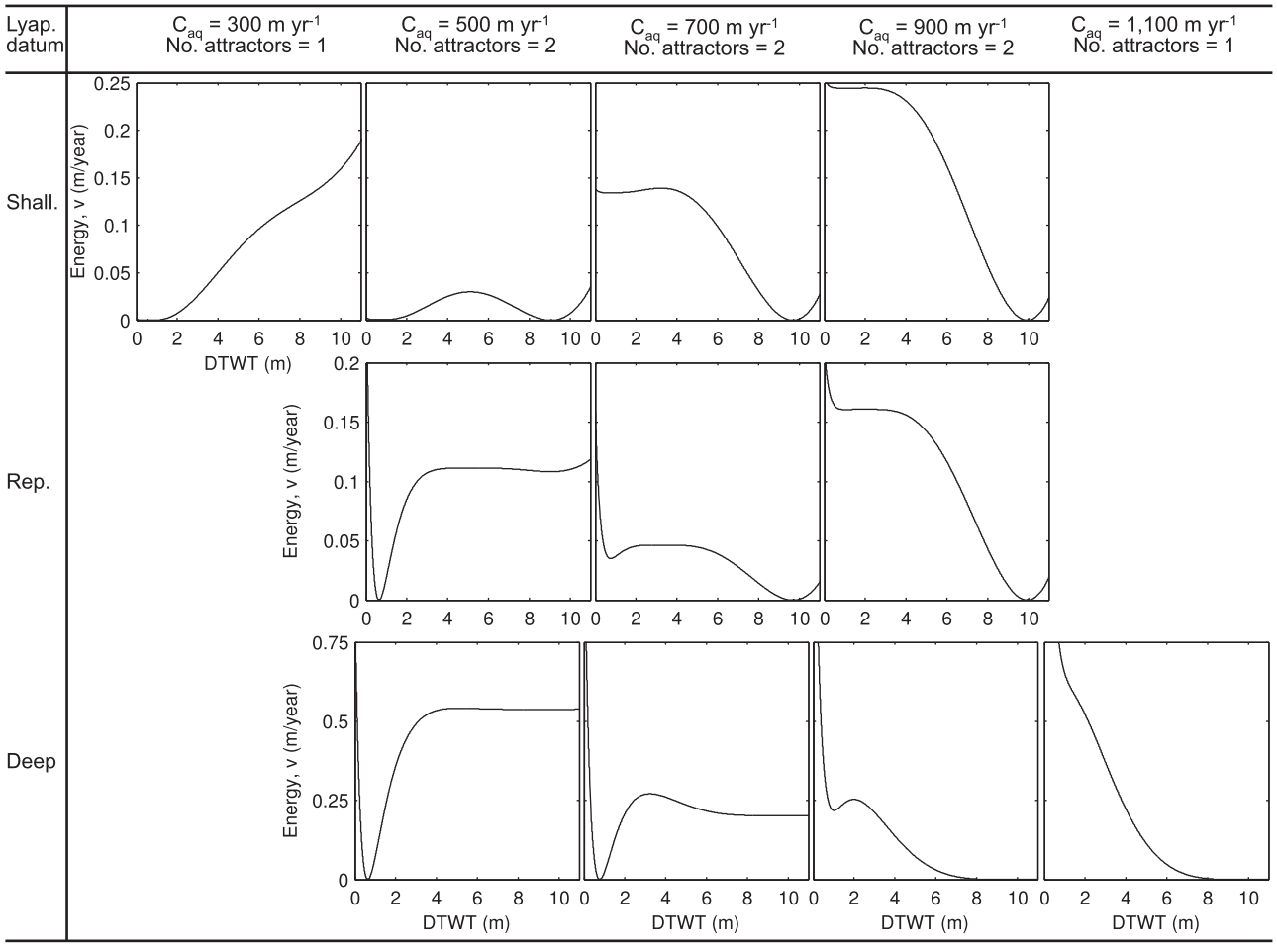

Figure 7. Lyapunov stability curves for depth to water table (DTWT) at five aquifer conductance parameter, C_{aq}, values repeated from three equilibrium datums where: *Shall.* denotes from the shallow attractor; *Rep.* denotes from the repellor; and *Deep* denotes from the deep attractor.

larger number of shallow attractor basin contours within Figure 3 at C_{aq} of 700 m yr^{-1}. This aspect only emerged when the datum was set to the deep attractor. Considering that the deep attractor is also the state to which the system would converge if no positive feedback existed, the deep attractor datum Lyapunov stability curves are the most plausible.

3.5. Assessing Stochastic Model Dynamics

[43] In this section, the behavior of the model under stochastic forcing is considered. Figure 8a shows the two stochastic time series of precipitation, which differ only in their standard deviation. Figure 8b shows time series of the depth to water table resulting from input of the precipitation series into the model (with C_{aq} set to 700 m yr^{-1}). Each hydrograph shows a switch from the shallow water table attractor basin to the deep attractor within the first 50 years; after which series *A* switched briefly back to the shallow attractor basin while series *B* persisted within the deep attractor, thus indicating it to be asymptotically stable (i.e., with sufficient time the model will converge to this attractor basin). The persistence within the deep attractor, and the rapid switching out of the shallow attractor, indicates the deep attractor to be significantly more resilient than the shallow attractor. However, the steady state forcing simulations (Figure 4) and Lyapunov stability plot from the deep attractor datum and C_{aq} at 700 m yr^{-1} (Figure 7) clearly indicate the shallow attractor to be the most resilient.

[44] This contradiction can be explained by better understanding what the Lyapunov stability plots are estimating and their use of climate forcing data. Importantly, the Lyapunov curves summarize the model dynamics when the forcing is set to a constant rate, in this case the mean annual precipitation. Therefore, the Lyapunov stability curve must be interpreted as the rate at which the system recovers to an attractor, following a disturbance, when it experiences only the constant rate of forcing. In no way can it characterize the displacement resulting from, or the resilience to, stochastic forcing input to the model. With regard to equilibrium continuation, for applications like those in Figure 5 that investigate a nonforcing parameter, the state-space distance from an attractor to the repellor cannot be interpreted as the resilience to stochastic forcing input to the model. Like Lyapunov stability curves, this state-space distance can only be interpreted as the cumulative impact from a disturbance not input to the model that the system can withstand before switching attractor basins. For this model, such disturbances would include groundwater pumping or

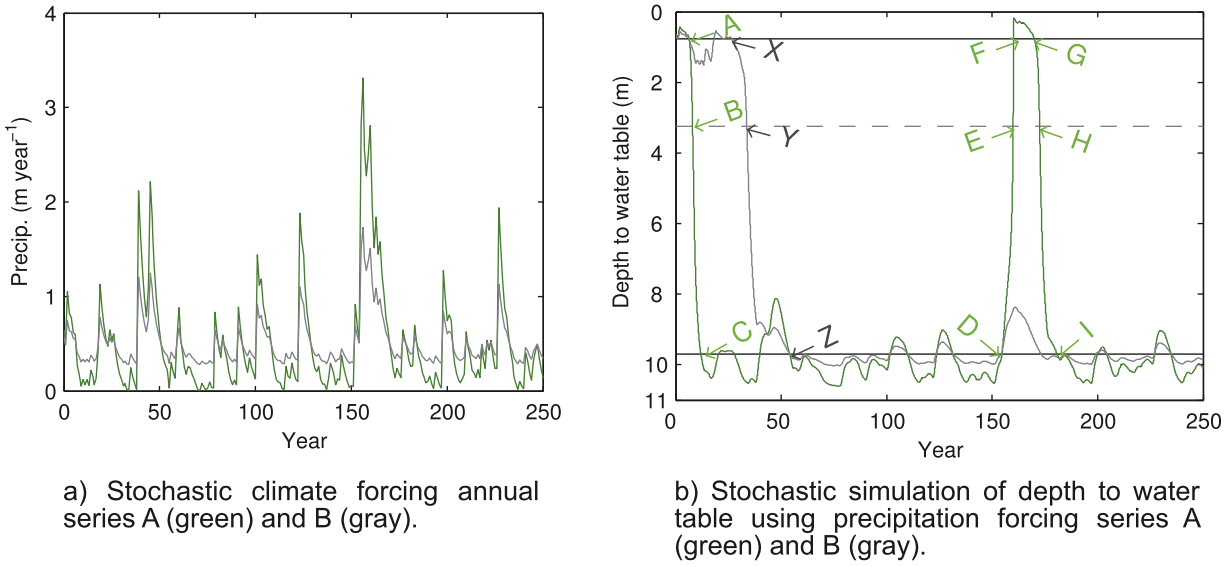

a) Stochastic climate forcing annual series A (green) and B (gray).

b) Stochastic simulation of depth to water table using precipitation forcing series A (green) and B (gray).

Figure 8. Model simulations from two stochastic precipitation series. The simulations show switching between the two attractors. Within Figure 8b, the solid horizontal lines denote attractors, the upper line designating a shallow attractor and the lower line a deep attractor; the dashed horizontal line denotes the repellor. The points on the green line (*A*-*I*) refer to data for series *A*; those on the gray line (*X*-*Z*) refer to data from series *B*.

flooding recharge. This is an important, but rarely considered, weakness of equilibrium continuation for resilience analysis; and even when equilibrium continuation has been undertaken for the forcing, the mechanism by which a switching of basins occurs has been unclear [*Guttal and Jayaprakash*, 2007; *Peterson*, 2009].

[45] To explore the mechanism by which stochastic forcing does cause a change of attractor basins, Figure 9 shows the 3-D Lyapunov stability surface for a range of annual precipitation rates and depth to water table (with C_{aq} set to 700 m yr^{-1}). Overlain is also the equilibrium continuation curve for the precipitation rate and the stochastic model simulations from Figure 8, with the corresponding points of an attractor basin change or repellor crossing also denoted. With regard to the surface, the gradient relative to the depth to water table axis shows how the depth to water table will change for a given rate of precipitation. The discontinuity at a precipitation of 1.35 m yr^{-1} is a numerical artifact of the methods. For precipitations less than 1.35 m yr^{-1}, the Lyapunov curve was calculated from a datum at the deep attractor, whereas for precipitations greater than 1.35 m yr^{-1} it was calculated from the shallow attractor because that is the only existent attractor for those precipitation rate (when C_{aq} equals 700 m yr^{-1}). Importantly, this threshold does not cause hysteresis; that is, at the deep attractor, high precipitation can cause a crossing of this threshold and lower precipitation can cause a reversal.

[46] With the stochastic forcing overlain, for series *A* and *B* it can be seen that the system is initially within the shallow attractor basin but after a period of low rainfall the lower limit to the shallow attractor is exceeded and, in year 6 (point *B*) and year 26 (point *Y*) for series *A* and *B*, respectively, each shifts toward the deep attractor. Each series arrives at the deep attractor in year 12 (point *C*) and year 54 (point *Z*), respectively, and series *A* remains within the deep attractor for 141 years while series *B* persists within it for the remaining duration of simulation. In year 154, a period of high rainfall shifts series *A* to a state having only the shallow attractor (point *D*). As this wet period is of sufficient duration, series *A* converges to the shallow attractor (point *F*) in year 160. Once within the shallow attractor basin, it only switches back to the deep attractor basin during a period of sufficiently low rainfall to shift the system to a state having only the deep attractor (points *G* and *H*). Overall, the transition of series *A* from point *A* to point *I* indicates that the existence of two attractors produces a counterclockwise hysteresis loop. Furthermore, counter to what much of the resilience literature implies, this indicates that the system does not switch between attractor basins by crossing the repellor. This process of attractor switching is likely to apply to other systems experiencing stochastic forcing of an additive or multiplicative form (see *Guttal and Jayaprakash* [2007] for a description of forcing types).

[47] Identification of this mechanism of attractor basin switching raises the question of whether two attractors can still emerge despite the system being parameterized to have only one attractor (according to equilibrium continuation). For this model, Figure 3 predicts only one attractor exists when C_{aq} equals 1100 m yr^{-1}. To investigate if multiple attractors can still emerge when C_{aq} equals 1100 m yr^{-1}, Figure 10a shows model simulation results derived using stochastic forcing of sufficiently high standard deviation to produce three periods of crossing from the deep attractor basin to the approximate depth of the shallow attractor. Figure 10b shows the equilibrium continuation plot for the annual precipitation rate on the *x* axis. The stochastic forcing overlain onto Figure 10b clearly shows the same counterclockwise hysteresis loop as in Figure 9. However, combined with the continuation plot, two differences are apparent. First, Figure 10b shows the lower limit of the

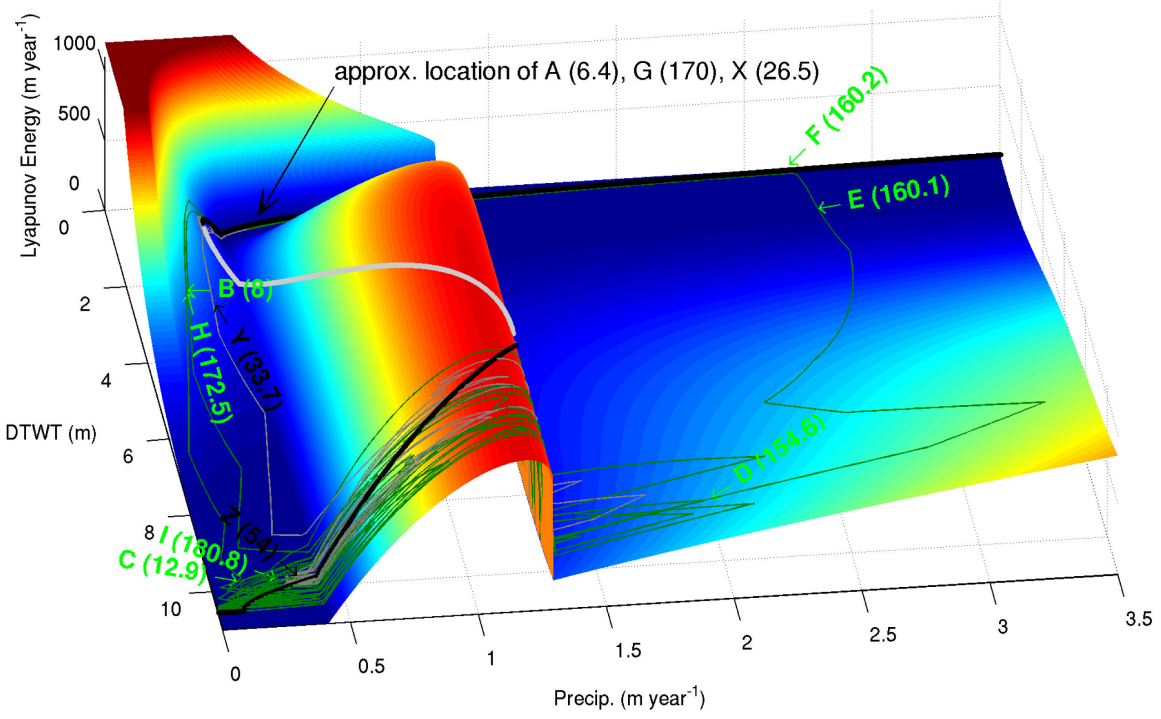

Figure 9. Attractor basin shape for precipitation and depth to water table (DTWT) derived using Lyapunov stability functions from the deep attractor datum with an aquifer conductance parameter, C_{aq}, of 700 m yr^{-1}. In the top left, Lyapunov energy values above 1200 m yr^{-1} were capped to 1200 m yr^{-1}. Note, the solid thick black line denotes an attractor; the solid thick gray line denotes a repellor; the thin solid green line denotes simulations from stochastic climate series *A*; and the thin solid gray line denotes simulations from stochastic climate series *B*. Series *A* is shown to have a counterclockwise hysteresis loop whereby the system starts within the shallow attractor (point *A*); a dry period shifts it to a state having only the deep attractor (point *C*); and after 141 years a wet period shifts the system back to the shallow attractor (points *D* to *F*). Points *A-I* and *X-Z* are as discussed in Figure 8 and the accompanying text. The color of the 3-D surface illustrates the quantity of Lyapunov energy marked on the vertical axis.

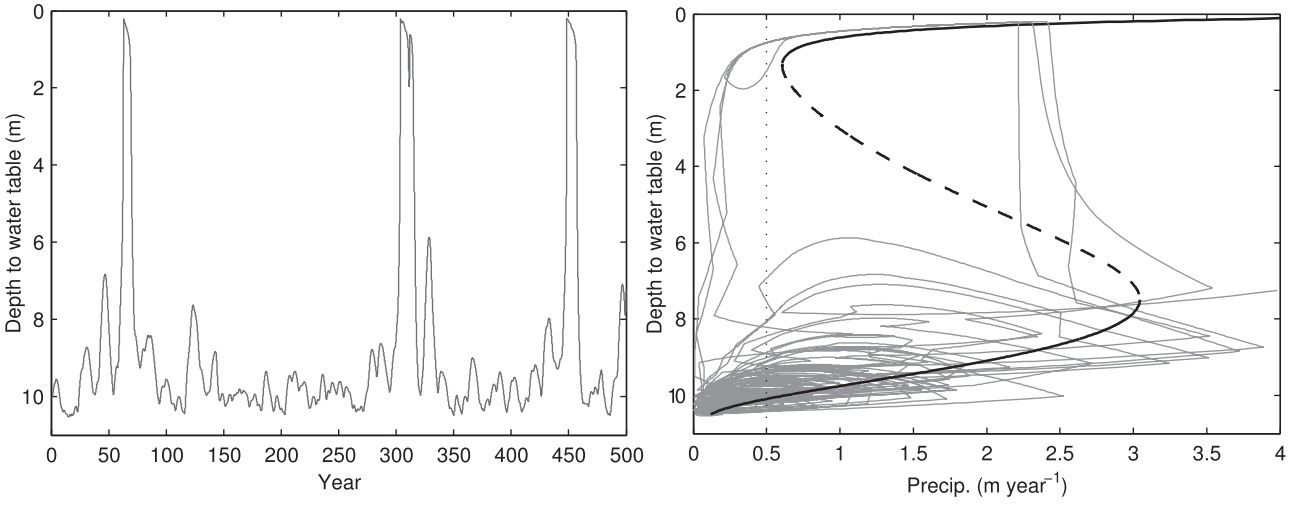

a) Stochastic simulation of depth to water table using a stochastic precipitation series derived with a standard deviation of 750 mm year^{-1} .

b) Equilibrium continuation for precipitation rate (black lines) with the stochastic simulation of depth to water table overlain (gray lines).

Figure 10. Demonstration of temporary attractor basin switching at a value of C_{aq} (1100 m yr^{-1}) which Figure 5 indicates has only one attractor. In Figure 10b, the solid thick black line denotes an attractor the dashed thick black line a repellor, the solid thin gray line the stochastic simulation of depth to water table from Figure 10a, and the vertical dotted line the mean annual precipitation of 0.5 m yr^{-1}.

two-attractor range to have shifted to a higher rate of precipitation such that at the mean precipitation of 0.5 m yr^{-1} only the deep attractor exists. This explains why Figure 3 shows only one attractor to exist at C_{aq} of 1100 m yr^{-1}. As shown by the overlain simulation, if the water level is within the shallow attractor basin, once the forcing returns to and persists at the mean rate, the water level will switch to the deep attractor. Therefore any transition into the shallow attractor basin is temporary, and very likely to be of a shorter duration than if two attractors existed at the mean rate of forcing. The second difference apparent in Figure 10b is a shift of the upper precipitation fold point to a significantly higher rate. Under stochastic forcing, a greater rate is therefore required to cause a switch to the shallow attractor; which explains why a larger standard deviation for the forcing series was required to produce a switching of attractors. It is interesting that two of the three switches to the shallow attractor occurred by crossing the repellor. This demonstrates that the forcing need not exceed the upper fold point to switch attractor basins but simply be near to it, which is probably related to the very low sensitivity of the Lyapunov energy surface with respect to depth to water table (as is seen for C_{aq} of 700 m yr^{-1} in Figure 9). A similar counterclockwise hysteresis loop is still evident in these cases.

[48] With regard to broader resilience science concepts, Figure 10 shows equilibrium continuation (when the x axis parameter is not the forcing rate) to be an inadequate means for identifying multiple attractors within systems with stochastic forcing. Use of such a method would fail to identify the switch to an alternative attractor which, while temporary, may be of sufficient duration relative to management concerns to be deemed significant. It also means that the controls on behavior of systems with multiple attractors may be misinterpreted.

[49] By undertaking equilibrium continuation for the forcing rate, two new insights are available. First, the likely attractor dynamics under stochastic forcing of a given mean and variance can be estimated by considering if an extreme forcing event(s) would be sufficient to cause an exceedance of a fold point. If neither fold point is likely to be exceeded then the system is unlikely to enter an alternate attractor basin, making the existence of multiple attractors somewhat inconsequential. If only one of the fold points is likely to be exceeded then the system will likely display asymptotic stability whereby the system will eventually converge to the attractor basin for which forcing is insufficient to cause an exit. If both fold points are likely to be exceeded then both attractors will be nonasymptomatic and the system will most likely repeatedly switch between the two attractor basins. Using this framework the implications from a change in the forcing mean or variance on the emergence of multiple attractors could also be explored without undertaking stochastic simulations.

[50] The second insight is that this framework provides a new measure of resilience that, unlike the equilibrium continuation of Figure 5, is consistent with the stochastic nature of the system. For considering the resilience to stochastic forcing endogenous to the model, the resilience of an attractor is best quantified as the difference between the mean forcing rate and the forcing at the fold point. Figure 11 demonstrates this measure for five values of aquifer conductance. For C_{aq} of 500 m yr^{-1}, it shows the deep and shallow attractor basins to be of near equal resilience. For C_{aq} of 700 and 900 m yr^{-1}, it shows the deep attractor basin to be significantly more resilient than the shallow attractor basin. However, for values of C_{aq} at which the mean forcing is, say, below the left fold point (e.g., the deep attractor when C_{aq} equals 1100 m yr^{-1}) this measure of resilience is inadequate for it would estimate zero resilience and fail to capture the likely transient switching to the attractor above the fold point (as shown to occur in Figure 10). For such instances, a probabilistic measure of resilience would be required that jointly considers the magnitude and probability of the relevant forcing events.

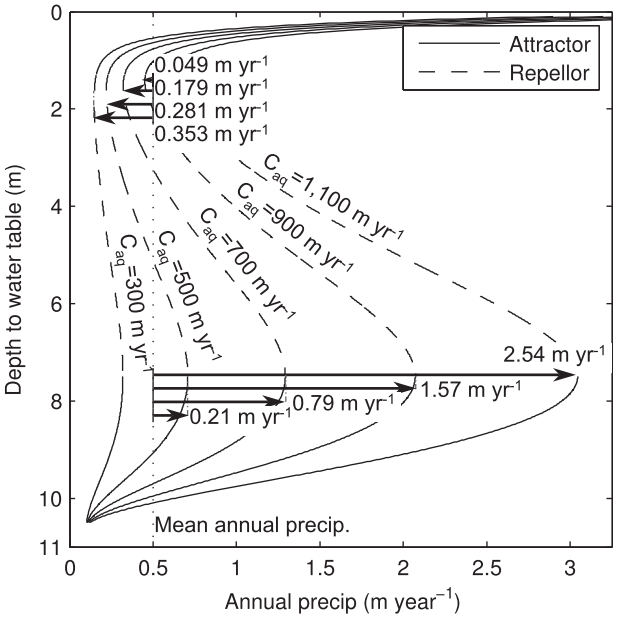

Figure 11. Resilience of each attractor to annual precipitation forcing (in units of annual precipitation rate) at five values of aquifer conductance parameter, C_{aq}.

[51] Often resilience studies are interested in the resilience to a transient disturbance that is not simulated within the model but may cause a switching of attractor basins. For this model, such disturbances would include groundwater pumping or flood recharge. To quantify the resilience to such an exogenous disturbance, the resilience of an attractor can be quantified by the standard measure of the state-variable distance from the attractor to the repellor. However, a more informative measure would be a Lyapunov stability curve for a specified constant forcing rate. In addition to providing the standard measure of resilience, its estimate of the *depth* of an attractor basin would inform the ease with which an exogenous disturbance could shift the system from an attractor and the rate of recovery after the exogenous disturbance. To jointly estimate the resilience to both endogenous and exogenous disturbances and for a single parameter set, a 3-D Lyapunov surface similar to Figure 9 may be useful.

4. Conclusions

[52] This paper attempts to advance the analytical resilience methods from *Ludwig et al.* [1997] within a hydrological context. More advanced continuation methods were

demonstrated and methods novel to resilience studies were proposed. Using a simple 1-D groundwater model, methods were demonstrated for (1) detecting attractors using time-integration simulations; (2) quantifying the state-space location of attractors and repellors with a change in one model parameter; and (3) quantifying the parameter space (in two dimensions) in which two attractors exist. In an effort to understand the model dynamics under stochastic forcing, methods were then developed to quantify the shape of each attractor basin using Lyapunov stability functions. Subtle aspects of implementation, such as the attractor datum, were discussed but more significantly the estimated attractor basin *depth* was found to be inconsistent with simulations based on stochastic climate forcing.

[53] To investigate this inconsistency, a 3-D Lyapunov stability surface was derived for a range in the precipitation forcing rate, and these results were overlain with stochastic model simulation results. This illustrated that the switch between attractor basins does not occur by crossing of the repellor but by exceedance of the precipitation rate at which two attractors exist (i.e., the exceedance of the fold points). This mechanism of switching should facilitate use of recently developed leading indicators of an imminent switching of attractors [*Biggs et al.*, 2009; *Guttal and Jayaprakash*, 2009; *Dakos et al.*, 2010]. The state-space distance from an attractor to a repellor was also shown to be an invalid measure of the resilience to stochastic forcing appearing within the model equations. Furthermore, the widely used method of equilibrium continuation under a constant forcing rate was shown to be an unreliable measure for quantifying the number of attractors. This was because temporary switching to a second attractor could occur at parameter values outside of the equilibrium continuation two-attractor range.

[54] To overcome these deficiencies, the resilience of a system to stochastic forcing was found to be best estimated by equilibrium continuation undertaken for the forcing rate rather than for a model parameter. In addition to explaining the switching between attractors, this measure also explained the common occurrence of a system able to switch from one attractor to a second but not back to the original attractor (i.e., asymptotic stability). Drawing from these findings, a new measure of resilience was proposed whereby the resilience to a forcing rate within the model is estimated as the difference between the mean rate and that at the fold point and the resilience to a disturbance outside of the model estimated by a Lyapunov stability curve with a constant forcing rate. While these measures do advance resilience science concepts, it is however unclear (1) how the forcing equilibrium continuation could be implemented when the annual forcing must be downscaled to, say, a monthly or daily time scale, as is a common requirement within hydrology; and (2) how a spatial dimension can be incorporated into the proposed Lyapunov stability curves.

[55] In closing, hydrological resilience is an emerging field of research. This paper has shown how a simple hydrological model can exhibit complex dynamics (in contrast to the many complex hydrological models that exhibit simple dynamics), and has detailed a number of techniques for exploration of such complex dynamics. However, most ecosystem resilience models are considerably more complex than the model investigated here, often comprising numerous coupled nonlinear differential equations. For such models, some of the analytical techniques proposed within this paper will not be applicable. It is hoped, however, that the insights gained from this paper will be of value to models of any complexity. Furthermore, more physically plausible hydrological resilience models are clearly required to lend weight to the theory of catchments having multiple steady states. It is hoped that the insights presented here will also provide a basis for such future investigations.

[56] **Acknowledgments.** The authors are grateful for the support received from the Australian Research Council (grant number: LP0991280), the Department of Sustainability and Environment, Victoria, Australia; the Department of Primary Industries, Victoria, Australia; and the Bureau of Meteorology, Australia. The Australian Research Council Linkage grant LP0455338 also provided support for the development of the material within sections 2.1, 2.3, and 2.4. The authors are also grateful for the considered review by Peter A. Troch and a second anonymous reviewer.

References

Anderies, J. M. (2005), Minimal models and agroecological policy at the regional scale: an application to salinity problems in southeastern Australia, *Reg. Environ. Change*, *5*(1), 1–17, doi:10.1007/s10113-004-0081-z.

Anderies, J. M., P. Ryan, and B. H. Walker (2006), Loss of resilience, crisis, and institutional change: Lessons from an intensive agricultural system in southeastern Australia, *Ecosystems*, *9*(6), 865–878, doi:10.1007/s10021-006-0017-1.

Asbjornsen, H., et al. (2011), Ecohydrological advances and applications in plant-water relations research: A review, *J. Plant Ecol.*, *4*(1–2), 3–22, doi:10.1093/jpe/rtr005.

Biggs, R., S. R. Carpenter, and W. A. Brock (2009), Turning back from the brink: Detecting an impending regime shift in time to avert it, *Proc. Natl. Acad. Sci.*, *106*(3), 826–831, doi:10.1073/pnas.0811729106.

Corless, R. M., G. H. Gonnet, D. E. G. Hare, D. J. Jeffrey, and D. E. Knuth (1996), On the Lambert w function, *Adv. Comput. Math.*, *5*, 329–359.

Dakos, V., E. H. van Nes, R. Donangelo, H. Fort, and M. Scheffer (2010), Spatial correlation as leading indicator of catastrophic shifts, *Theor. Ecol.*, *3*(3), 163–174, doi:10.1007/s12080-009-0060-6.

Dent, C. L., G. S. Cumming, and S. R. Carpenter (2002), Multiple states in river and lake ecosystems, *Philos. Trans. R. Soc. London Ser. B*, *357*(1421), 635–645, doi:10.1098/rstb.2001.0991.

Dhooge, A., W. Govaerts, and Y. A. Kuznetsov (2003), MATCONT: A MATLAB package for numerical bifurcation analysis of ODEs, *ACM Trans. Math. Softw.*, *29*(2), 141–164.

D'Odorico, P., and A. Porporato (2004), Preferential states in soil moisture and climate dynamics, *Proc. Natl. Acad. Sci. U.S.A.*, *101*(24), 8848–8851.

D'Odorico, P., F. Laio, and L. Ridolfi (2005), Noise-induced stability in dryland plant ecosystems, *Proc. Natl. Acad. Sci. U.S.A.*, *102*(31), 10,819–10,822, doi:10.1073/pnas.0502884102.

D'Odorico, P., F. Laio, L. Ridolfi, and M. Lerdau (2008), Biodiversity enhancement induced by environmental noise, *J. Theor. Biol.*, *255*(3), 332–337.

D'Odorico, P., V. Engel, J. Carr, S. Oberbauer, M. Ross, and J. Sah (2011), Tree-grass coexistence in the everglades freshwater system, *Ecosystems*, *14*(2), 298–310, doi:10.1007/s10021-011-9412-3.

Guttal, V., and C. Jayaprakash (2007), Impact of noise on bistable ecological systems, *Ecol. Modell.*, *201*(3–4), 420–428, doi:10.1016/j.ecolmodel.2006.10.005.

Guttal, V., and C. Jayaprakash (2009), Spatial variance and spatial skewness: Leading indicators of regime shifts in spatial ecological systems, *Theor. Ecol.*, *2*(1), 3–12, doi:10.1007/s12080-008-0033-1.

Heffernan, J. (2008), Wetlands as an alternative stable state in desert streams, *Ecology*, *89*(5), 1261–1271.

Hilt, S., J. Kohler, H. P. Kozerski, E. H. van Nes, and M. Scheffer (2011), Abrupt regime shifts in space and time along rivers and connected lake systems, *Oikos*, *120*(5), 766–775, doi:10.1111/j.1600-0706.2010.18553.x.

Holling, C. S. (1973), Resilience and stability of ecological systems, *Ann. Rev. Ecol. Syst.*, *4*, 1–23, doi:10.1146/annurev.es.04.110173.000245.

Kuznetsov, Y. A. (2004), *Elements of Applied Bifurcation Theory*, 3rd ed., vol. 22, 631 pp., Springer, New York.

Ludwig, D., B. H. Walker, and C. S. Holling (1997), Sustainability, stability, and resilience, *Conserv. Ecol.*, *1*(1), 7. [Available at http://www.consecol.org/vol1/iss1/art7/.]

Lyapunov, A. M. (1992), The general problem of the stability of motion, *Int. J. Control*, *55*(3), 531–773, doi:10.1080/00207179208934253. [English translation of Lyapunov A.M. (1892) The general problem of the stability of motion (in Russian), doctoral dissertation, Univ. Kharkov].

May, R. M. (1977), Thresholds and breakpoints in ecosystems with a multiplicity of stable states, *Nature*, *269*(5628), 471–477.

Møller, J. K., J. Carstensen, H. Madsen, and T. Andersen (2009), Dynamic two state stochastic models for ecological regime shifts, *Environmetrics*, *20*(8), 912–927, doi:10.1002/env.962.

Peterson, T. J. (2009), Multiple hydrological steady states and resilience, Ph.D. thesis, Department of Civil and Environmental Engineering, Univ. of Melbourne, Melbourne, Australia. [Available at http://repository.unimelb.edu.au/10187/8540.]

Peterson, T. J., R. M. Argent, A. W. Western, and F. H. S. Chiew (2009a), Multiple stable states in hydrological models: An ecohydrological investigation, *Water Resour. Res.*, *40*, W03406, doi:10.1029/2008WR006886.

Peterson, T. J., A. W. Western, and R. M. Argent (2009b), Multiple hydrological stable states and the probability of climate variability causing a threshold crossing, in *18th IMACS World Congress and MODSIM09 International Congress on Modelling and Simulation*, edited by R. Anderssen, R. Braddock, and L. Newham, pp. 3109–3115, Modell. and Simul. Soc. of Aust. and N.Z. and Int. Assoc. for Math. and Comput. in Simul., Cairns, Australia.

Rennermalm, A. K., J. M. Nordbotten, and E. F. Wood (2010), Hydrologic variability and its influence on long-term peat dynamics, *Water Resour. Res.*, *46*, W12546, doi:10.1029/2009WR008242.

Ridolfi, L., P. D'Odorico, and F. Laio (2006), Effect of vegetation-water table feedbacks on the stability and resilience of plant ecosystems, *Water Resour. Res.*, *42*, W01201, doi:10.1029/2005WR004444.

Rodriguez-Iturbe, I., P. D'Odorico, F. Laio, L. Ridolfi, and S. Tamea (2007), Challenges in humid land ecohydrology: Interactions of water table and unsaturated zone with climate, soil, and vegetation, *Water Resour. Res.*, *43*, W09301, doi:10.1029/2007WR006073.

Runyan, C., and P. D'Odorico (2010), Ecohydrological feedbacks between salt accumulation and vegetation dynamics: Role of vegetation-groundwater interactions, *Water Resour. Res.*, *46*, W11561, doi:10.1029/2010WR009464.

Sastry, S. (1999), *Nonlinear System: Analysis, Stability, and Control*, 667 pp., Springer, New York.

Scheffer, M., S. R. Carpenter, J. A. Foley, C. Folke, and B. H. Walker (2001), Catastrophic shifts in ecosystems, *Nature*, *413*(6856), 591–596.

Serizawa, H., T. Amemiya, and K. Itoh (2009), Noise-triggered regime shifts in a simple aquatic model, *Ecol. Complexity*, *6*(3), 375–382, doi:10.1016/j.ecocom.2009.03.002.

Shampine, L., and M. Reichelt (1997), The MATLAB ODE suite, *SIAM J. Sci. Stat. Comput.*, *18*(1), 1–22.

Srikanthan, R., G. Kuczera, M. Thyer, and T. McMahon (2002), Stochastic generation of annual climate data, *Tech. Rep. 02/6*, Cooperative Res. Cent. for Catchment Hydrology, Melbourne, Australia.

van de Koppel, J., and M. Rietkerk (2004), Spatial interactions and resilience in arid ecosystems, *Am. Nat.*, *163*(1), 113–121.

van Nes, E. H., and M. Scheffer (2005), Implications of spatial heterogeneity for catastrophic regime shifts in ecosystems, *Ecology*, *86*(7), 1797–1807.

von Hardenberg, J., E. Meron, M. Shachak, and Y. Zarmi (2001), Diversity of vegetation patterns and desertification, *Phys. Rev. Lett.*, *87*(19), 198101.

Walker, B. H., C. S. Holling, S. R. Carpenter, and A. Kinzig (2004), Resilience, adaptability and transformability in social-ecological systems, *Ecol. Soc.*, *9*(2), 5. [Available at http://www.ecologyandsociety.org/vol9/iss2/art5/.]